Journal of Biomechanics 45 (2012) 832–841

Contents lists available at SciVerse ScienceDirect

Journal of Biomechanics

journal homepage: www.elsevier.com/locate/jbiomech
www.JBiomech.com

Modeling of cardiac muscle thin films: Pre-stretch, passive and active behavior

Jongmin Shim [a,*], Anna Grosberg [b], Janna C. Nawroth [c], Kevin Kit Parker [b], Katia Bertoldi [a,*]

[a] School of Engineering and Applied Science, Harvard University, Cambridge, MA, United States
[b] Disease Biophysics Group, Wyss Institute for Biologically Inspired Engineering, School of Engineering and Applied Science, Harvard University, Cambridge, MA, United States
[c] Division of Biology, California Institute of Technology, Pasadena, CA, United States

ARTICLE INFO

Article history:
Accepted 4 October 2011

Keywords:
Cardiomyocytes
Cell alignment
Bio-hybrid thin film
Constitutive model
Finite element simulation
Pre-stretch
Isometric twitch stress

ABSTRACT

Recent progress in tissue engineering has made it possible to build contractile bio-hybrid materials that undergo conformational changes by growing a layer of cardiac muscle on elastic polymeric membranes. Further development of such muscular thin films for building actuators and powering devices requires exploring several design parameters, which include the alignment of the cardiac myocytes and the thickness/Young's modulus of elastomeric film. To more efficiently explore these design parameters, we propose a 3-D phenomenological constitutive model, which accounts for both the passive deformation including pre-stretch and the active behavior of the cardiomyocytes. The proposed 3-D constitutive model is implemented within a finite element framework, and can be used to improve the current design of bio-hybrid thin films and help developing bio-hybrid constructs capable of complex conformational changes.

1. Introduction

The field of tissue engineering is rapidly moving toward rebuilding living tissues and organs through the development of stem-cell-derived cells and *in vitro* manufacturing of extracellular matrix proteins (Place et al., 2009). Organs and tissues adopt complex 3-D configurations and dynamics, so the capability to model the conformation of engineered tissues is essential for their design. Contractile bio-hybrid materials have been built by growing a monolayer of spatially aligned cardiac myocytes on synthetic elastomeric thin films (Feinberg et al., 2007). When the bio-hybrid film is released into solution and electrically stimulated, the myocytes contract, forcing the construct into adopting a 3-D conformation (Feinberg et al., 2007; Alford et al., 2010). The development of such muscular thin films (MTFs, *i.e.*, a rectangular construct actuated by aligned cardiomyocytes) for building actuators and powering devices requires exploring several design parameters which include the arrangement of the cardiac myocytes and the thickness and Young's modulus of the elastomeric film.

Finite element (FE) analysis provides an efficient way to explore those design parameters, and it will allow researchers to create contractile constructs with non-trivial 3-D geometries (*e.g.*, flexible pumps). Such modeling capability could play an important role in designing constructs that would finish their building process, or self-assembly *in vivo*. Additionally, it could greatly aid in the development of *in vitro* assays to test pharmaceutical agents for efficacy and toxicity as well as evaluation of stem-cell-derived tissues. For example, a completed FE model which includes fluid–MTF coupling would allow quantification of the resistance experienced by the films at different field frequency and more accurate evaluation of the effect of chronotropic drugs.

Along with the advances in tissue engineering, constitutive models have been proposed to investigate the behavior of anisotropic bio-materials (Spencer, 1984; Weiss et al., 1996) and skeletal muscle (Blemker et al., 2005; Böl and Reese, 2008; Calvo et al., 2010). Cardiac muscle is, like skeletal muscle, characterized by highly organized striated myofibrils; however, it also exhibits spontaneous activity as well as mechanical, chemical, and electrical cell-to-cell coupling (functional syncytium) leading to through-conduction of impulses and, subsequently, a highly synchronous response. Recently, a few researchers (Sainte-Marie et al., 2006; Sermesant et al., 2006; Chapelle et al., 2010) proposed physiology-based models for cardiomyocytes, which considers the mechanism of the involuntary contractile behavior of cardiac muscle due to the action potential under calcium flux and captures the characteristic energy dissipative process of the cardiomyocyte active contribution. However, those physiology-based models are mathematically complex and the identification of the model parameters is very challenging. To overcome these difficulties, Böl et al. (2009) proposed a phenomenological model, which neglects the energy dissipation of the active contribution,

* Corresponding authors.
E-mail addresses: jshim@seas.harvard.edu (J. Shim), bertoldi@seas.harvard.edu (K. Bertoldi).

0021-9290/$ - see front matter © 2011 Elsevier Ltd. All rights reserved.
doi:10.1016/j.jbiomech.2011.11.024

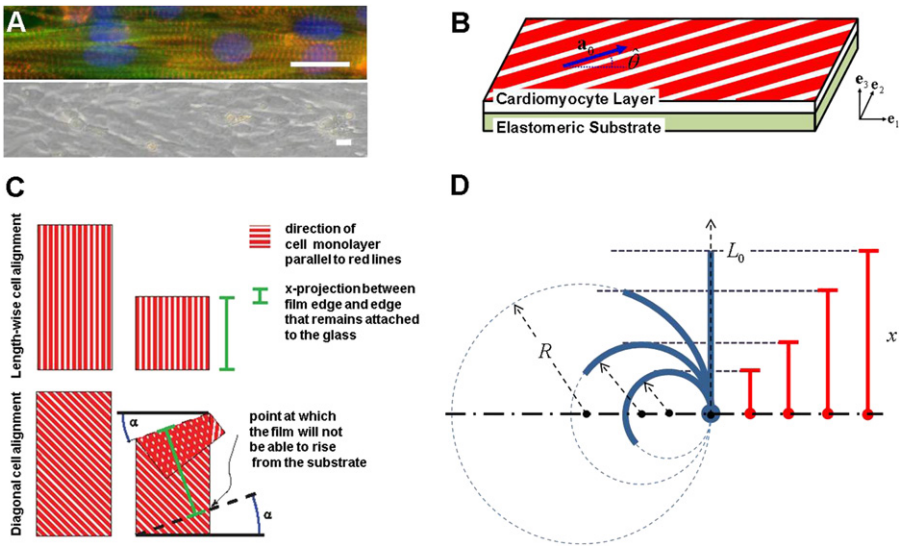

Fig. 1. (A) Top: intracellular alignment of sarcomeres having nuclei (blue), actin (green), alpha-actinin (red). Bottom: a bright-field image of the same tissue showing the overall alignment of cells in the tissue. The length of both scale bars represent 20 μm. (B) Schematic of the muscular thin film (MTF). Here, $\mathbf{a_0}$ and $\hat{\theta}$ represent the cell alignment vector and the corresponding angle, respectively. (C) Schematic showing the projection of the MTF with length-wise cell alignment (top) and with diagonal cell alignment (bottom). The x-projection is indicated in green and α in blue. (D) Schematic of MTF illustrating the geometric relation of x, L_0 and R in Eq. (1). (For interpretation of the references to color in this figure legend, the reader is referred to the web version of this article.)

leading to a formulation where parameter identification is much easier.

A successful constitutive model of cardiac muscle should capture the active behavior including both systole and diastole and the passive behavior including pre-stretch deformation of the muscle cells[1] and provide an efficient procedure for model parameter identification. Although Böl et al. (2009) successfully modeled the active behavior of cardiac muscle cells on thin films using 1-D truss-type elements, their model is not able to predict the pre-stretched deformation observed in unconstraint MTFs. Currently there is no phenomenological model capable of capturing all those features. Here, we propose a 3-D phenomenological constitutive model which accounts for both the passive thin film deformation including pre-stretch during cell maturation as well as the active behavior of the cardiac muscle cells. The proposed constitutive model is implemented within a FE framework and used to simulate the experimental results of diastolic and systolic conformations in MTFs. Particularly, in order to accommodate the variation in mechanical properties observed in cultured cardiac tissue, a range of values is identified for both the induced pre-stretch and the isometric twitch stress.

This paper is organized as follows: the experiments for parameter identification and model validation are described in Section 2. In Section 3, the constitutive model is presented for both the elastomeric silicone layer and the cardiac muscle layer. Section 4 demonstrates the model parameter identification results based on literature and experiments with length-wise cell alignment on films. As a validation of the proposed model, Section 5 shows comparison between the numerical and experimental results for constructs with diagonal cell alignment. In addition, parametric studies are also presented to investigate the influence of the thin film thickness, isometric twitch stress, and pre-stretch deformation on MTF conformational changes.

2. Experiments with bio-hybrid films

This section briefly describes the experiments used for identifying parameters and validating the model, and experimental details and methods are provided in Section S1 of the supporting material. Briefly, polydimethylsiloxane (PDMS, Sylgard 184-Dow Corning, Midland, MI) thin films have extracellular matrix proteins, fibronectin patterned on their surface by microcontact printing. Ventricular myocytes from neonatal rats are chemically dissociated and seeded onto the PDMS, where they bind to the fibronectin and self-organize into an anisotropic monolayer whose tissue architecture reflects the orientation of the patterned extracellular matrix (Fig. 1A). The resulting bio-hybrid material is a cantilevered beam anchored to the surface of the two dimensional culture dish (Fig. 1B). During systole, the contracting cell layer would induce a bending deformation in the MTF normal to the plane of the dish (Fig. 1C). To provide the simplest possible deformation geometry to fit the model parameters, the cells were aligned parallel to the MTF length (*length-wise*) (Fig. 1C, top), and the deformation was a simple bending with a constant radius of curvature throughout the MTF. To validate the model with more complex kinematics, we also built chips with *diagonal* alignment of myocytes on the MTF (Fig. 1C, bottom). During the experiments, the MTF's kinematics was recorded with a high speed camera through a stereomicroscope, and the resultant movies depicted the projection of the films on the substrate plane. The curvature or the radius of curvature were calculated from the projection data and used to quantitatively compare experimental and simulation results (Fig. 1D).

2.1. Experiments for parameter identification and model validation

We tested the contractile response of MTFs with three different PDMS thickness (*i.e.*, 14.5 μm, 18.0 μm, 23.0 μm) for the constructs with length-wise cell alignment and single PDMS

[1] In the following, we will refer to "active" behavior when describing magnitude and time course of stresses and MTF (*i.e.*, a rectangular construct actuated by aligned cardiomyocytes) deformation resulting from cardiomyocytes contraction. These strains and stresses are increasing during the systolic phase until peak systole is reached, and are decreasing during diastole until a fully relaxed state is attained. However, even at this fully relaxed state, MTF curvature might be present due to the pre-stress of the cells, and resulting pre-stretch of the substrate, introduced during tissue maturation. These pre-stresses and strains that are present even at the fully relaxed state will be referred to as "passive" behavior.

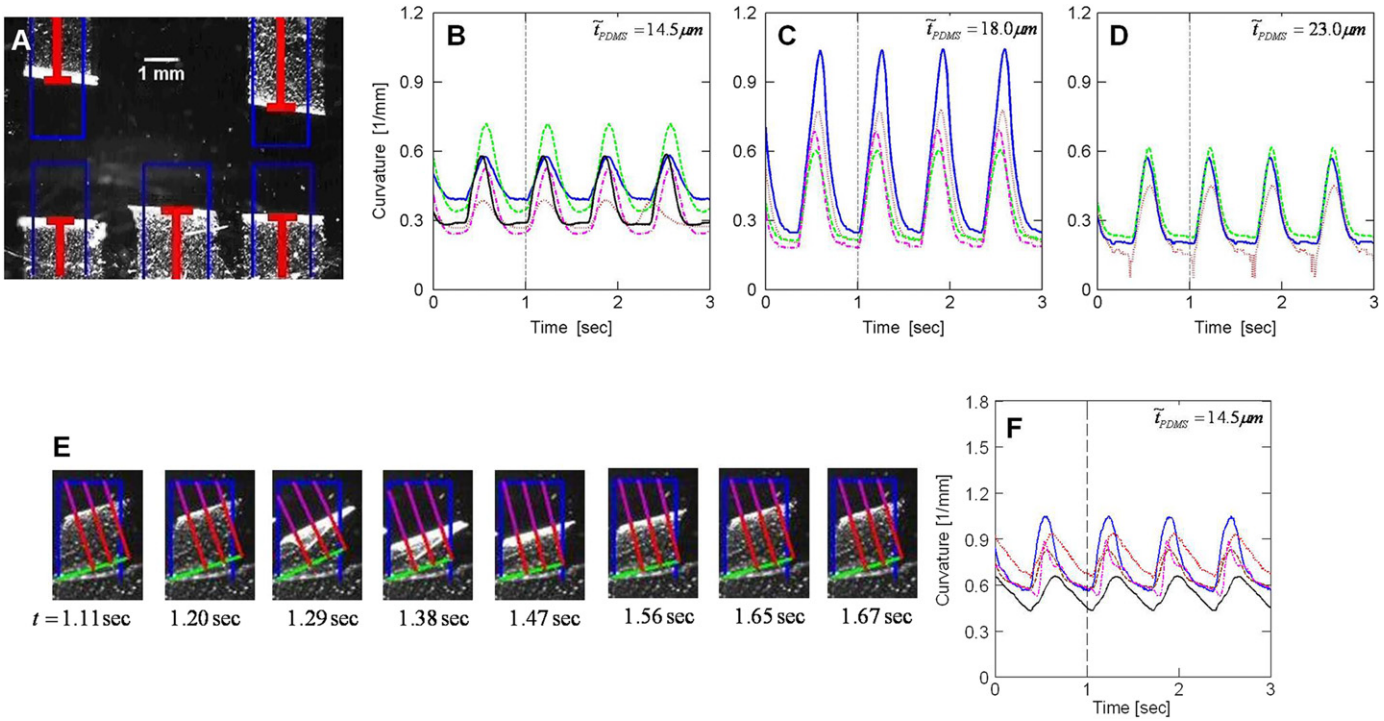

Fig. 2. Experimental results from MTFs with length-wise cell alignment (A–D) and with diagonal cell alignment (E and F). (A) Brightfield image of contractile behavior of MTFs with length-wise cell alignment (PDMS thickness of 14.5 μm) taken at $t=1.215$ s. The red line represents the projection length (x in Eq. (1), and the blue line denotes the original film length (L_0 in Eq. (1)). (B–D) Time–curvature plots for MTFs with length-wise cell alignment. Curvature plots for all films on each chip with three different PDMS thicknesses, *i.e.*, (B) $\tilde{t}_{PDMS}=14.5$ μm, (C) $\tilde{t}_{PDMS}=18.0$ μm, and (D) $\tilde{t}_{PDMS}=23.0$ μm. (E) Snapshots of contractile behavior MTF with diagonal cell alignment (PDMS thickness of 14.5 μm). The green line marks the border of the portion of the film lying on glass. The blue line denotes the film when it is completely flat on the glass. The length of the red segment corresponds to x in Eq. (1), while the sum of the lengths of the purple segment and red segment is L_0 in Eq. (1). (F) Time–curvature plots for MTFs with diagonal cell alignment (PDMS thicknesses of $\tilde{t}_{PDMS}=14.5$ μm). (For interpretation of the references to color in this figure legend, the reader is referred to the web version of this article.)

thickness (*i.e.*, 14.5 μm) for the constructs with diagonal cell alignment case. Test results for the length-wise cell alignment case are presented in Fig. 2A–D. The experiments were conducted on MTF chips with multiple films on every chip (see Fig. 2A) to replicate the biological variance while constraining engineering variables such as PDMS thickness and cell alignment. The time–curvature plots are presented in Fig. 2B–D. Similarly, Fig. 2E and F summarizes test results from diagonal cell alignment case. Diagonal cell alignment MTFs were also studied on multi-film chips to isolate any biological variations. Indeed, a non-negligible variation of the time–curvature plots under identical experimental conditions can be easily observed. In these experiments, the field stimulated films contracted out of the culture plane as depicted schematically in Fig. 1 and the projection of the MTF tracked with customized software. During diastole, the cells return to their rest length, and the MTF recoils to the rest position. The cyclic bending of the films during 1.5 Hz stimulation is repeatable and several cardiac cycles worth of data was measured for analysis.

2.2. Data analysis

We assume that the deformed shape of the film is described by the arc of a circle, so that the curvature of the film, K, can be calculated by measuring the projection length x and following the simple relation:

$$x=\begin{cases} R\sin\left(\dfrac{L_0}{R}\right) & \text{if } x>\dfrac{L_0}{\pi}, \\ R & \text{if } x\le\dfrac{L_0}{\pi}, \end{cases} \tag{1}$$

where $R=1/K$ is the radius of curvature, and L_0 is the longitudinal length of MTF. The geometric relation of x, L_0 and R is shown in Fig. 1D.

After the experiments were completed the data movies were filtered to remove noise, made binary using image processing software (ImageJ, NIH), and processed using MatLab (Mathworks, Natick, MA) to calculate the curvature of the film. For the case of length-wise cell alignment, the MTF curvature is obtained from the measured projection length, by directly applying Eq. (1). However, with diagonal cell alignment case, due to the non-trivial conformation of the bio-hybrid film, a more elaborated procedure was developed. A parameter, α, is defined as the angle between the film's free and fixed edges (see Fig. 1C (bottom)). We define the base of the film as the line marking the border between the portion of the film lying on the glass and the free section (black dashed line in Fig. 1C). The x-projection length is defined as the distance between the base of the film and the free edge of the film (green solid line in Fig. 1C). Then, the average of temporal MTF curvature (*i.e.*, the prevailing curvature of the MTF) was obtained by minimizing the standard deviation of the temporal curvature collection calculated along the bottom edge of the film. In order to have consistent comparison between the FE model and the experimental results, the movies produced in the simulations and experiments were analyzed using the same software.

3. Constitutive modeling of bio-hybrid films

This section highlights the key components of the proposed constitutive model; its detailed derivation is provided in Section S2 of the supporting material.

Let $\mathbf{F}=\partial\mathbf{x}/\partial\mathbf{X}$ be the deformation gradient mapping a material point from the reference position $\mathbf{X}$ to its current position $\mathbf{x}$, and $J=\det\mathbf{F}$ be its determinant. The behavior of nearly incompressible materials is effectively described by splitting the deformation locally into volumetric (denoted by superscript v) and isochoric (denoted by superscript i) components as

$$\mathbf{F}=\mathbf{F}^{v}\cdot\mathbf{F}^{i},\quad \text{where } \mathbf{F}^{v}=J^{1/3}\mathbf{1},\quad \mathbf{F}^{i}=J^{-1/3}\mathbf{F}. \tag{2}$$

3.1. Elastomeric substrate

The elastomeric substrate is fabricated using PDMS, and its behavior is well captured using a neo-Hookean model. Based on the kinematic assumption shown in Eq. (2) with $\mathbf{C}^{i}=\mathbf{F}^{i^{T}}\cdot\mathbf{F}^{i}$ and $\bar{I}_1=\mathrm{tr}\mathbf{C}^{i}$, a decoupled form of the strain energy density (Gurtin et al., 2010) is given by

$$\psi=\psi^{v}(J)+\psi^{i}(\bar{I}_1)=\frac{\tilde{\kappa}}{2}(J-1)^2+\frac{\tilde{E}}{6}(\bar{I}_1-3), \tag{3}$$

where $\tilde{\kappa}$ and $\tilde{E}$ denote the bulk modulus and the initial elastic modulus of the elastomer, respectively. The Cauchy stress $\mathbf{T}$ is found by differentiating ψ with respect to $\mathbf{C}$, yielding

$$\mathbf{T}=\tilde{\kappa}(J-1)\mathbf{1}+\frac{\tilde{E}}{3J}\mathrm{dev}(\mathbf{B}^{i}). \tag{4}$$

where $\mathbf{B}^{i}=\mathbf{F}^{i}\cdot\mathbf{F}^{i^{T}}$ and "dev" stands for deviatoric part of 2nd order tensors.

3.2. Cardiac muscle cells

The characteristic energy dissipative process of the cardiomyocyte active contribution can be captured by recently developed physiology-based models, which consider the mechanism of the involuntary contractile behavior of cardiac muscle due to the action potential under calcium flux (Sainte-Marie et al., 2006; Sermesant et al., 2006; Chapelle et al., 2010). However, this approach is mathematically complex, and model parameter identification is challenging. In this article, instead, we take a simple, but effective phenomenological approach, neglecting the energy dissipative process. While recently Böl et al. (2009) developed a phenomenological model for cardiac muscle cells, their formulation neglects the important effect of the pre-stretch that the muscle cells develop as they mature. This paper presents a 3-D phenomenological model that captures the two major features of cardiac muscles: the passive behavior including pre-stretched deformation and their active behavior including systole and diastole.

Kinematics including pre-stretch. Even when resting, muscle cells *in vivo* experience a state of stress due to their pre-stretched conditions. This can be clearly observed from the experimental data reported in Fig. 2B–D and F, showing a non-negligible MTF curvature during diastole. In order to account for such pre-stretched conditions, previous constitutive models introduced an *ad hoc* strain-shift in the stress–strain curve (Blemker et al., 2005; Böl et al., 2009; Calvo et al., 2010) leading to a non-unique material response that depends on the level of pre-stretch of muscle cells. However, such formulation does not capture the non-negligible MTF curvature observed during diastole. Thus, in this paper, a different approach is adopted to model pre-stretch; inspired by the multiplicative decomposition introduced by Kroner (1960) and Lee (1969), the isochoric deformation gradient $\mathbf{F}^{i}$ in Eq. (2) is decomposed into load-induced, $\mathbf{F}^{iL}$, and pre-stretched, $\mathbf{F}^{iS}$, contributions

$$\mathbf{F}^{i}=\mathbf{F}^{iL}\cdot\mathbf{F}^{iS}. \tag{5}$$

Here, for the sake of simplicity, the pre-stretch is assumed to be fully developed during cell differentiation and maturation prior to the experiment, and not to be affected by the cell active response. If we also assume that the pre-stretch deformation is incompressible and the cells deform affinely, the pre-stretched contribution to the deformation gradient $\mathbf{F}^{iS}$ is given by

$$\mathbf{F}^{iS}=\mathbf{Q}\boldsymbol{\Lambda}\mathbf{Q}^{T}, \tag{6}$$

with

$$\boldsymbol{\Lambda}=\hat{\lambda}_S\mathbf{e}_1\otimes\mathbf{e}_1+(\hat{\lambda}_S)^{-1/2}(\mathbf{e}_2\otimes\mathbf{e}_2+\mathbf{e}_3\otimes\mathbf{e}_3), \tag{7}$$

$$\mathbf{Q}=\cos\hat{\theta}(\mathbf{e}_1\otimes\mathbf{e}_1+\mathbf{e}_2\otimes\mathbf{e}_2)+\sin\hat{\theta}(-\mathbf{e}_1\otimes\mathbf{e}_2+\mathbf{e}_2\otimes\mathbf{e}_1)+\mathbf{e}_3\otimes\mathbf{e}_3, \tag{8}$$

where $\hat{\lambda}_S$ is the pre-stretch induced into the cardiac myocytes lying in the x_1–x_2 plane during maturation (*i.e.*, myogenesis and tissue development) and $\hat{\theta}$ is the angle identifying the cell alignment in the undeformed configuration (see Fig. 1B). The diastole curvatures of the experimental data reported in Fig. 2B–D and F clearly show a deviation in the pre-stretched response of the cells as a result of the diversity in cell conditions. Therefore, we expect the parameter $\hat{\lambda}_S$ not to be uniquely determined, but to be influenced by experimental factors such as, but not limited to, small variations in temperature/humidity, local density variations, local intracellular architecture, and cardiac origin of the cells (left or right ventricle).

Constitutive equations for passive and active behavior. When an isotropic material is reinforced by a family of fibers with direction $\mathbf{a}_0=\cos\hat{\theta}\mathbf{e}_1+\sin\hat{\theta}\mathbf{e}_2$ in the reference configuration (Fig. 1B), the isochoric part of the strain energy can be expressed as a function of not only the invariants of $\mathbf{C}$, but also additional invariants depending on $\mathbf{a}_0$. To describe both passive (representing resting status) and active (including systole and diastole) behavior of cardiomyocytes, we specify a decoupled form of free energy as

$$\psi=\psi^{v}(J)+\psi^{i}_{iso}(\bar{I}_1)+\psi^{ip}_{ani}(\bar{I}_4)+\psi^{ia}_{ani}(\bar{I}_4,q), \tag{9}$$

where $\bar{I}_4=\mathbf{a}_0\cdot\mathbf{C}^{i}\cdot\mathbf{a}_0$ and q is the activation level of cardiac muscle cells. In the proposed model, while ψ^{v} and ψ^{i}_{iso} reflect the volumetric and the isotropic contributions of the intercellular part, respectively, ψ^{ip}_{ani} and ψ^{ia}_{ani} represent the passive and the active contributions of anisotropic effect of the myofibril, respectively. Their detailed forms can be found in Section S2 of the supporting material. By differentiating ψ with respect to $\mathbf{C}$, the resulting Cauchy stress for the cardiac muscle cells is obtained as

$$\mathbf{T}=\mathbf{T}^{v}+\mathbf{T}^{i}_{iso}+\mathbf{T}^{ip}_{ani}+\mathbf{T}^{ia}_{ani}, \tag{10}$$

where

$$\mathbf{T}^{v}=\hat{\kappa}(J-1)\mathbf{1}, \tag{11}$$

$$\mathbf{T}^{i}_{iso}=\frac{\hat{E}_c}{3J}\mathrm{dev}(\mathbf{B}^{i}), \tag{12}$$

$$\mathbf{T}^{ip}_{ani}=\frac{\hat{E}_p\bar{\lambda}}{\hat{\alpha}J}[e^{\hat{\alpha}(\bar{\lambda}-1)}-1]\mathrm{dev}(\bar{\mathbf{a}}\otimes\bar{\mathbf{a}}), \tag{13}$$

$$\mathbf{T}^{ia}_{ani}=\begin{cases}\dfrac{\hat{P}q}{J}\left[1-\left(\dfrac{\bar{\lambda}-\hat{\lambda}_o}{1-\hat{\lambda}_o}\right)^2\right]\mathrm{dev}(\bar{\mathbf{a}}\otimes\bar{\mathbf{a}}) & \text{if } 1<\bar{\lambda}<(2\hat{\lambda}_o-1),\\ 0 & \text{otherwise.}\end{cases} \tag{14}$$

Table 1
Summary of model parameters and their physical meaning.

PDMS	$\tilde{E}=1.5$ MPa	Initial elastic modulus
	$\tilde{\kappa}=25$ MPa	Initial bulk modulus
Cardiac muscle cell		
Pre-stretched	$\hat{\theta}=0^{\circ},30^{\circ}$	Angle defining the initial alignment of the cells within the x_1-x_2 plane
	$\hat{\lambda}_S \in [1.11,1.18]$	Pre-stretch developed in the cardiomyocytes during cell maturation
Volumetric	$\hat{\kappa}=380$ kPa	Initial bulk modulus
Isotropic	$\hat{E}_c=2.3$ kPa	Initial elastic modulus of intercellular part
Anisotropic Passive	$\hat{E}_p=21$ kPa	Initial elastic modulus of fiber
	$\hat{\alpha}=5.5$	Constant related to the slope of stress–strain relation of passive fiber
Anisotropic Active	$\hat{P} \in [2.8,21.6]$ kPa	Isometric twitch stress
	$\hat{\lambda}_o=1.24$	Optimal stretch for the maximum active stress
	$\hat{T}=0.21$ s	Characteristic time scale for contraction

Table 2
Summary of the model described in Section 3. Note that $g(\tau)$ is an arbitrary time history describing the cell pre-stretch development.

Given at time τ	$\mathbf{F}^{ABQ}(\tau)$: deformation gradient given by ABAQUS
Kinematics	$J(\tau)=\det\mathbf{F}^{ABQ}(\tau)$
	$\mathbf{F}^{v}(\tau)=J(\tau)\mathbf{1}$
	$\mathbf{F}^{iL}(\tau)=J(\tau)^{-1/3}\mathbf{F}^{ABQ}$
	$\mathbf{\Lambda}=\hat{\lambda}_S\mathbf{e}_1\otimes\mathbf{e}_1+(\hat{\lambda}_S)^{-1/2}(\mathbf{e}_2\otimes\mathbf{e}_2+\mathbf{e}_3\otimes\mathbf{e}_3)$
	$\mathbf{Q}=\cos\hat{\theta}(\mathbf{e}_1\otimes\mathbf{e}_1+\mathbf{e}_2\otimes\mathbf{e}_2)+\sin\hat{\theta}(-\mathbf{e}_1\otimes\mathbf{e}_2+\mathbf{e}_2\otimes\mathbf{e}_1)+\mathbf{e}_3\otimes\mathbf{e}_3$
	$\mathbf{F}^{iS}(\tau)=g(\tau)\mathbf{Q}\cdot\mathbf{\Lambda}\cdot\mathbf{Q}^{T}$
	$\mathbf{F}(\tau)=\mathbf{F}^{v}(\tau)\cdot\mathbf{F}^{iL}(\tau)\cdot\mathbf{F}^{iS}(\tau)$
Constitutive equation	$\mathbf{a_0}(\tau)=\cos\hat{\theta}\mathbf{e}_1+\sin\hat{\theta}\mathbf{e}_2$
	$\mathbf{C}^{i}(\tau)=\mathbf{F}^{i^T}(\tau)\cdot\mathbf{F}^{i^T}(\tau)$
	$\overline{\lambda}=\sqrt{\mathbf{a}_0\cdot\mathbf{C}^{i}\cdot\mathbf{a}_0}$
	$\mathbf{B}^{i}(\tau)=\mathbf{F}^{i}(\tau)\cdot\mathbf{F}^{i^T}(\tau)$
	$\overline{\mathbf{a}}(\tau)=\mathbf{F}^{i}(\tau)\cdot\mathbf{a}_0/\overline{\lambda}$
	$q(\tau)=\left(\frac{\tau}{\hat{T}}\right)^2\exp\left[1-\left(\frac{\tau}{\hat{T}}\right)^2\right]$
	$\mathbf{T}^{v}(\tau)=\hat{\kappa}(J(\tau)-1)$
	$\mathbf{T}^{i}_{iso}(\tau)=\frac{\hat{E}_c}{3J(\tau)}\mathrm{dev}(\mathbf{B}^{i}(\tau))$
	$\mathbf{T}^{ip}_{ani}(\tau)=\frac{\hat{E}_p\overline{\lambda}(\tau)}{\hat{\alpha}J(\tau)}[e^{\hat{\alpha}(\overline{\lambda}(\tau)-1)}-1]\mathrm{dev}(\overline{\mathbf{a}}(\tau)\otimes\overline{\mathbf{a}}(\tau))$
	$\mathbf{T}^{ip}_{ani}(\tau)=\begin{cases}\frac{\hat{P}q(\tau)}{J(\tau)}\left[1-\left(\frac{\overline{\lambda}(\tau)-\hat{\lambda}_o}{1-\hat{\lambda}_o}\right)^2\right]\mathrm{dev}(\overline{\mathbf{a}}(\tau)\otimes\overline{\mathbf{a}}(\tau)) & \text{if } 1<\overline{\lambda}(\tau)<(2\hat{\lambda}_o-1)\\ 0 & \text{otherwise}\end{cases}$
	$\mathbf{T}(\tau)=\mathbf{T}^{v}(\tau)+\mathbf{T}^{i}_{iso}(\tau)+\mathbf{T}^{ip}_{ani}(\tau)+\mathbf{T}^{ia}_{ani}(\tau)$

Here, $\overline{\lambda}=\sqrt{I_4}$, $\overline{\mathbf{a}}=\mathbf{F}^{i}\cdot\mathbf{a}_0/\overline{\lambda}$,

$$q(t)=\left(\frac{t}{\hat{T}}\right)^2\exp\left[1-\left(\frac{t}{\hat{T}}\right)^2\right], \tag{15}$$

and the physical meaning of all the model parameters (*i.e.*, $\hat{\kappa}$, $\hat{E_c}$, $\hat{E_p}$, $\hat{\alpha}$, $\hat{P}$, $\hat{\lambda}_o$, $\hat{T}$) is summarized in Table 1.

Model implementation. The constitutive model outlined in this section has been implemented into the commercial finite element code ABAQUS/Explicit, using a user-defined subroutine VUMAT, and Table 2 summarizes the model and its implementation. Each FE analysis consists of two steps: the fist step simulates the development of pre-stretch into the non-activated cells; in the second step, the active response of MTFs is simulated under fully pre-stretched conditions.

4. Model parameter identification

In this section, we present the procedure followed to identify the parameters entering in the constitutive model. Additional details are provided in Section S3 of the supporting material.

While the material parameters for the elastomeric substrate ($\tilde{E}=1.5$ MPa, $\tilde{\kappa}=25$ MPa) are provided by the manufacturers, the parameters needed to characterize the cardiac muscle cell response are obtained from the literature and contraction assays

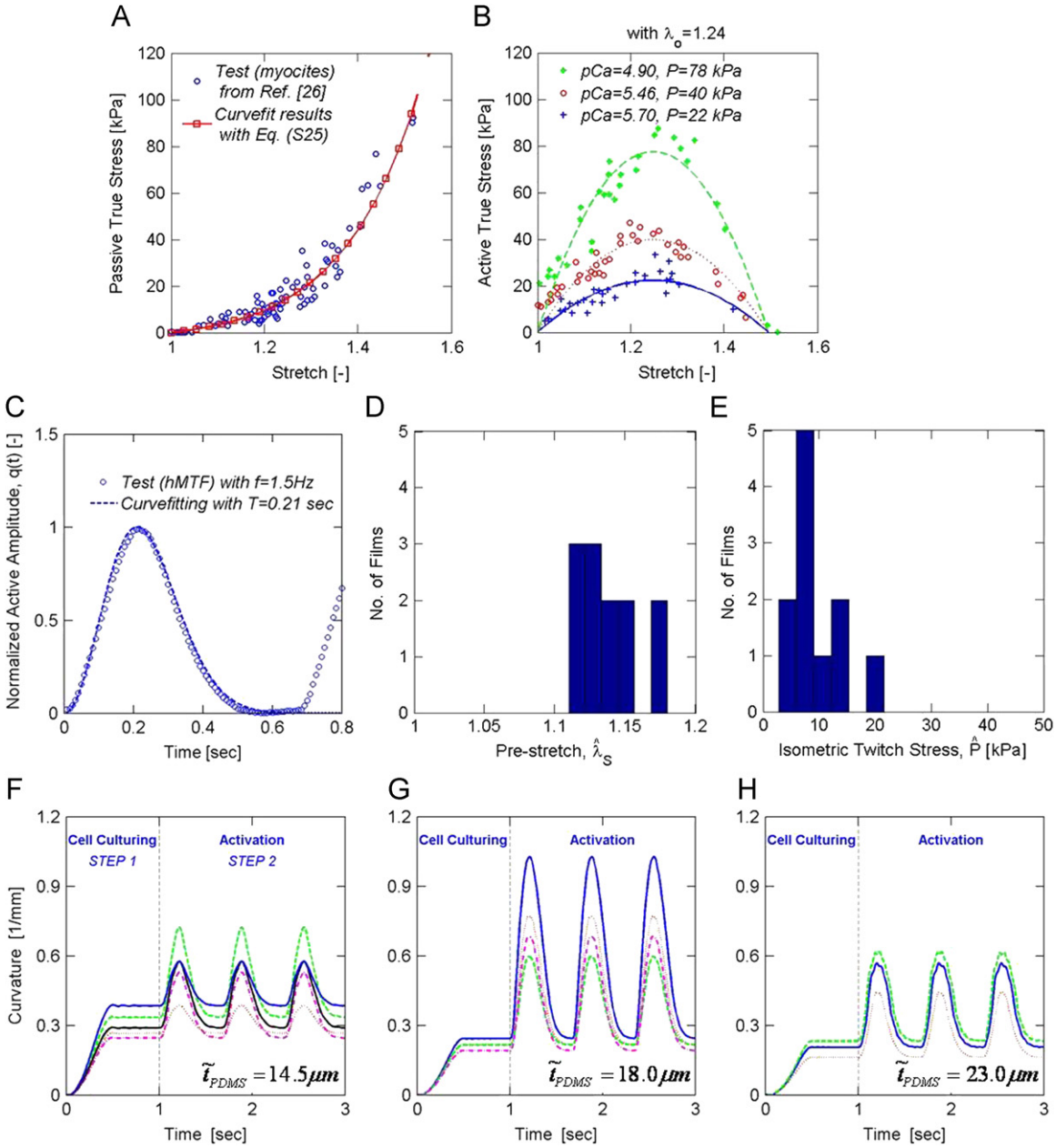

Fig. 3. Model parameter identification from Weiwad et al. (2000) (A and B) and from experiments with length-wise cell alignment (C–H). (A) Tensile behavior of non-activated cells. Blue circular markers denote experimental data and the red line corresponds to Eq. (S21). (B) Isometric twitch stress as a function of calcium concentration ($pCa = -\log_{10}(a_{Ca^{2+}})$). Markers denote experimental data and the lines correspond to Eq. (S21). (C) A typical profile of the active amplitude history from tests performed on MTFs with length-wise cell alignment. Markers denote experimental data, and the line corresponds to $q(t)$ in Eq. (15). (D and E) Range of values identified for $\hat{\lambda}_S$ and $\hat{P}$. (F–H) Time–curvature plots for MTFs with length-wise cell alignment from FE simulations. Note that one-to-one correspondence between experimental (Fig. 2B–D) and numerical (F–H of this figure) curves. (For interpretation of the references to color in this figure legend, the reader is referred to the web version of this article.)

performed with neonatal rat ventricular myocytes micropatterned on PDMS thin films.

4.1. Parameters identified from the literature

The paper by Weiwad et al. (2000) provides in a single article nearly all the required test results to identify the material parameters entering into the proposed material model. Moreover, all their data are in a good agreement with similar test results for the heart muscle of adult rats (*i.e.*, Granzier and Irving, 1995 and Palmer et al., 1996 for passive behavior and Nishimura et al., 2000 and Palmer et al., 1996 for active behavior). Thus, the test results presented in Weiwad et al. (2000) are used to identify five material-specific parameters entering into the proposed constitutive model.

From their tensile tests of the non-activated cells (shown in Fig. 3A), we determine three model parameters, *i.e.*, $\hat{E}_c = 21$ kPa, $\hat{E}_p = 2.3$ kPa, and $\alpha = 5.5$ by curve-fitting the test results with Eqs. (12) and (13) specialized to uniaxial loading conditions. Moreover, the experimental results obtained for the isometric twitch stress (Fig. 3B) guide us to propose a quadratic form of active stress profile as shown in Eq. (14), and determine $\hat{\lambda}_o = 1.24$. Finally, for the sake of simplicity, we assume that the cardiac muscle is nearly incompressible and its volumetric behavior is determined by the non-activated cell response, resulting in a bulk modulus of $\hat{\kappa} = 380$ kPa.

4.2. Parameters identified from MTF tests with length-wise cell alignment

Experiments with length-wise cell alignment are used to identify the remaining three model parameters ($\hat{P}$, $\hat{\lambda}_S$, $\hat{T}$). While $\hat{P}$ and $\hat{\lambda}_S$ are experimental-conditions-specific, $\hat{T}$ denotes the characteristic time scale of contractile behavior under the stimulating electric pulse. First, $\hat{T}=0.21$ s is identified by curve-fitting a typical profile of the active amplitude history shown in Fig. 3C with $q(t)$ in Eq. (15).

Secondly, values for both $\hat{\lambda}_S$ and $\hat{P}$ are determined using the experimental data presented in Fig. 2B–D. As in the experiments, MTFs with PDMS substrate of thickness $\tilde{t}=14.5$, 18.0, or 23.0 μm and cardiac myocytes thickness $\hat{t}=4$ μm are modeled and simulated. Since the experiments show a significant variability in the material response for each curvature history shown in Fig. 2B–D, both $\hat{\lambda}_S$ and $\hat{P}$ are determined to achieve the best fit while leaving all the other model parameters unchanged. Thus, a range of values is identified for $\hat{\lambda}_S$ and $\hat{P}$ whose distributions are shown in Fig. 3D and E, respectively. More specifically, we obtain (a) $\hat{\lambda}_S \in [1.11, 1.16]$ and $\hat{P} \in [2.8, 7.3]$ kPa for $\tilde{t}=14.5$ μm, (b) $\hat{\lambda}_S \in [1.12, 1.14]$ and $\hat{P} \in [9.2, 21.6]$ kPa for $\tilde{t}=18.0$ μm, and (c) $\hat{\lambda}_S \in [1.16, 1.18]$ and $\hat{P} \in [6.9, 8.5]$ kPa for $\tilde{t}=23.0$ μm. While a rather small variation in the pre-stretch ranging from $\hat{\lambda}_S=1.11$ to 1.18 is observed, we find a quite large variation in the isometric twitch stress ranging from $\hat{P}=2.7$ to 21.6 kPa. Finally, Fig. 3F–H reports the curvature histories of MTFs obtained from FE simulations, clearly showing that the model correctly capture the curvature induced by pre-stretch curvature during cell maturation and the active response.

5. Numerical simulation results

In this section, we first validate the proposed model by simulating MTFs with diagonal cell alignments, and then present a series of parametric studies to investigate the effect of PDMS thickness, isometric twitch stress, and pre-stretch of cells.

5.1. Model validation for MTFs with diagonal cell alignment

In order to validate the proposed model, the identified model parameters listed in Table 1 are used to simulate the behavior of MTFs with diagonal cell alignment. To incorporate the variation of cell conditions observed in MTFs with length-wise cell alignment, we perform simulations with two extreme sets of parameters: one with $\hat{\lambda}_S=1.11$ and $\hat{P}=2.8$ kPa (weakest cell conditions), and the other with $\hat{\lambda}_S=1.18$ and $\hat{P}=21.6$ kPa (strongest cell conditions). As shown in Fig. 4A and B, the FE simulations qualitatively capture the experimentally observed behavior (see Fig. 2E). In addition, Fig. 4C clearly shows that all the experimental time–curvature data are bounded by the simulation results obtained using two extreme cell conditions.

5.2. Parametric studies

Since the quantification of stresses within cells is experimentally challenging, inspired by Stoney's approximate plate analysis (Stoney, 1909) various formulations have been proposed to estimate stress from curvature measurements (Atkinson, 1995; Alford et al., 2010). Using the proposed 3-D constitutive model, FEM simulations can provide more accurate predictions for stress and strain distribution. Here, we explore the effect of important parameters within MTF with length-wise cell alignment (*e.g.*, the PDMS thickness, the isometric twitch stress of cells, and the pre-stretch of cells) on the stress history; additional details of the simulations are summarized in Section S4 of the supporting material.

Effect of PDMS thickness. The effect of PDMS thickness on the response of the MTFs is explored by varying $\tilde{t}$ from 13.0 μm to 28.0 μm. The average value of the two cell-condition-dependent parameters is used (*i.e.*, $\hat{\lambda}_S=1.14$ and $\hat{P}=9.0$ kPa), while keeping all other parameters unchanged.

Fig. 5A shows the effect of PDMS thickness on the average of maximum principal stress within the cardiac cells, denoted by $\overline{S}$. In order to obtain $\overline{S}$, we collect the time history of the maximum principal stress within all the cardiac cell elements, and then calculate the spatial average. It is interesting to observe that the results of the FEM simulations show a negligible effect of the PDMS thickness on the cells stress. To better quantify this behavior, we decompose $\overline{S}$ into the passive contribution ($\overline{S}_p$) and the active contribution ($\overline{S}_a$),

$$\overline{S}=\overline{S}_p+\overline{S}_a, \tag{16}$$

and plot their maximum values ($\max(\overline{S}_p)$, $\max(\overline{S}_a)$) separately in Fig. 5B, confirming no effect of the PDMS thickness on the cells stress.

Effect of isometric twitch stress of cells. In the experiments, we observe that the active response of cells largely changes from test to test. In the proposed model, such variation in the cell response

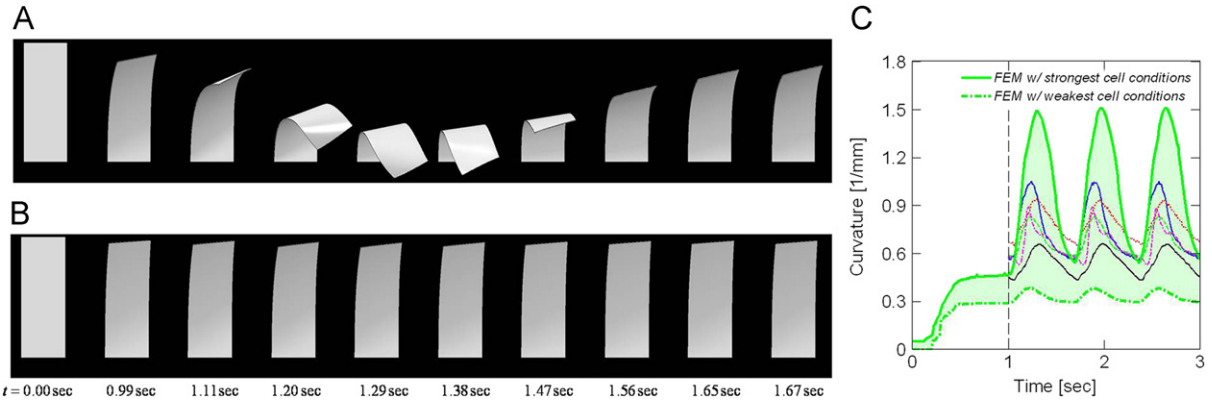

Fig. 4. Contractile behavior of MTF with diagonal cell alignment (PDMS thickness of 14.5 μm) from FE simulations. (A) Snapshots of FE simulation with strongest cell conditions (*i.e.*, pre-stretch of $\hat{\lambda}_S=1.18$ and isometric twitch stress of $\hat{P}=21.6$ kPa). (B) Snapshots of FE simulation with weakest cell conditions (*i.e.*, pre-stretch of $\hat{\lambda}_S=1.11$ and isometric twitch stress of $\hat{P}=2.8$ kPa). (C) Comparison of experimental and numerical time–curvature plots. The green shaded region corresponds to the area bounded by simulations with two extreme cell conditions considered in this study. (For interpretation of the references to color in this figure legend, the reader is referred to the web version of this article.)

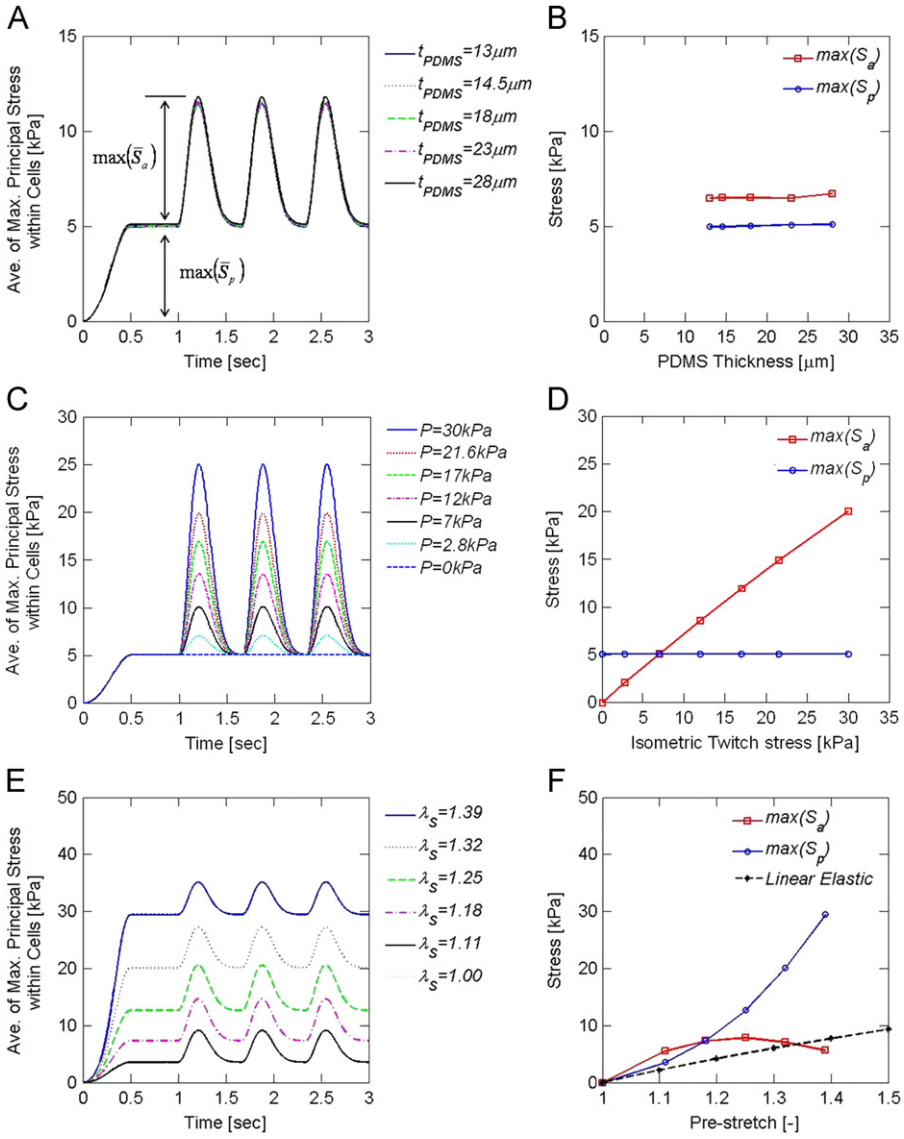

Fig. 5. FE parametric studies: the left column for the averaged histories of maximum principal stress ($\bar{S}$), and right column for the stress contribution of passive and active response ($\max(S_p)$ and $\max(S_a)$). (A and B) Effect of PDMS thickness, (C and D) effect of isometric twitch stress of cells, (E and F) effect of cell pre-stretch.

can be studied by exploring the value of the isometric twitch stress, $\hat{P}$. We vary $\hat{P}$ from 0 to 30.0 kPa while keeping all other parameters unchanged, including $\tilde{t}=18.0$ μm and $\hat{\lambda}_S=1.14$. The effect of $\hat{P}$ on the MTF response is reported in Fig. 5C and D, showing that the active stress within the cells increases linearly with the isometric twitch stress, as formulated in Eq. (2).

Effect of cell pre-stretch. It is well known that the pre-stretch within the cells is largely affected by the substrate and the mechanical/chemical stimulus during maturation (Wang et al., 2002; Griffin et al., 2004; Engler et al., 2008). We investigate systematically the effect of pre-stretch ($\hat{\lambda}_S$); the effect of pre-stretch on the cardiomyocyte response is investigated by varying $\hat{\lambda}_S$ from 1.00 (*i.e.*, no pre-stretch) to 1.39 while keeping all other parameters unchanged and using $\tilde{t}=18.0$ μm and $\hat{P}=9.0$ kPa.

The results are reported in Fig. 5E and F, they indicate that a linear model, $\overline{S}_{linear}=(\hat{E}_c+\hat{E}_p)\ln\hat{\lambda}_S$, poorly captures the stress distribution within the cells. Moreover, it is interesting to observe that the case with no pre-stretch (*i.e.*, $\hat{\lambda}_S=1.00$) results in no stress within the cells. Finally, the simulations also show an exponential form of the stretch-stress relation for the passive fiber response and a quadratic relation for the active fiber response. Note that because of the quadratic relation between the pre-stretch and the active stress contribution, we observe an optimal pre-stretch value at which a maximum level of active response (*i.e.*, maximum active mobility) is achieved.

6. Discussion and conclusions

6.1. Discussion

In this paper, we investigate through experiments and simulations the response of MTFs with length-wise and diagonal cell alignments. First, we establish a simple procedure based on the measured projection length to quantify the curvature of MTFs with both length-wise and diagonal cell alignments. The proposed method allows, for the first time, quantification of the curvature of MTFs with diagonal cell alignment, suggesting that the procedure can be extended to the analysis of constructs with non-trivial shapes such as swimmers. In order to simulate and predict the observed experimental behavior of MTFs, we propose a 3-D phenomenological constitutive model that captures the passive film deformation

including pre-stretch as well as the active behavior of cardiomyocytes. Inspired by the multiplicative decomposition introduced by Kroner (1960) and Lee (1969), the isochoric deformation gradient is decomposed into load-induced and pre-stretched contributions so that the effect of the pre-stretch can be independently investigated. To simplify the identification of parameters entering in the model, we propose a phenomenological formulation where the cardiomyocyte active contribution is described by an elastic model and all the different aspects of constitutive behaviors are decoupled. Data from literature and experiments conducted on MTFs with length-wise cell alignment are used to identify all the model parameters. Moreover, the variation in mechanical properties observed during experiments is accounted for by identifying a range of values for the induced pre-stretch ($\hat{\lambda}_S$) and the isometric twitch stress ($\hat{P}$). The resulting formulation captures qualitatively and quantitatively the experimentally observed response of MTFs with diagonal cell alignment. MTFs are characterized by a very complicated chemo-mechanical behavior. To capture the salient features of their response with a sufficiently simple formulation, several assumptions need to be made: here, the energy dissipating mechanism is neglected and a decoupled form of free energy is adopted.

Recently proposed physiology-based constitutive models consider the mechanism of the involuntary contractile behavior of cardiac muscle due to the action potential under calcium flux (Sainte-Marie et al., 2006; Sermesant et al., 2006; Chapelle et al., 2010). These formulations capture the characteristic energy dissipative process of the cardiomyocyte active contribution and satisfy the thermodynamics laws. However, these models are mathematically complex and lead to sophisticated procedures for the identification of the model parameters (Sermesant et al., 2006), making unrealistic the use of such models as design tools for MTF actuators. Instead, we take a simple, but effective phenomenological approach in the spirit of Blemker et al. (2005) and Böl et al. (2009), where the energy dissipative behavior of the active contribution is neglected. To describe the active response of cardiomyocytes, an elastic model is adopted and a scalar internal variable (q in Eq. (15)) is introduced, leading to a formulation that does not satisfy the free energy imbalance conditions.

Several theories for metal plasticity (Brown et al., 1989), approximately incompressible elastic materials (Anand, 1996), and fiber-reinforced composite (Spencer, 1984) are based on a separable form of free energy (the so-called *separability hypothesis* Gurtin et al., 2010) and consider separately the contributions of plastic, volumetric and anisotropic deformation. This formulation provides an effective way to incorporate various aspect of the complex material behavior into a relatively simple model. Inspired by this approach, we decouple all the aspects of the muscle response (see Eq. (9)) although there is no experimental evidence for such assumption. However, this formulation leads to a substantially simplified procedure for the identification of the model parameters; most of them can be identified from literature, and only a few need to be identified from reference experiments.

6.2. Conclusions

We present a 3-D phenomenological constitutive model that captures the passive film deformation including pre-stretch during cell maturation as well as the active behavior of the cardiac muscle cells. While a range of values is identified for two model parameters (induced pre-stretch $\hat{\lambda}$ and isometric twitch stress $\hat{P}$) to account for the variation in mechanical properties observed in experiments, all other model parameters are obtained from the literature. The proposed model is implemented within a FE framework and used to simulate the experimental results of diastolic and systolic conformations in a muscular thin film. With the identified model parameters, the proposed model qualitatively captured the behavior of MTFs with diagonal cell alignment, and all the experimental time–curvature data are bounded by the numerical results obtained using two extreme cell conditions.

The proposed constitutive model can be immediately extended to the analysis of constructs with non-trivial 3-D initial geometries. This will greatly aid in the engineering of soft muscle-powered robots, but it will require a computationally efficient implementation of the model and the use of shell elements within the FE framework. Furthermore, the model has the potential to take into account fluid–structure interactions, opening avenues for the design of swimming constructs, actuators, and micro-fluidic devices.

Conflict of interest statement

The authors report that no conflicts of interest, financial or otherwise, influenced this work.

Acknowledgements

This work has been supported by the Harvard Materials Research Science and Engineering Center under NSF award number DMR-0820484 (KB), DMR-0213805 (KKP), and NIH grant 1 R01 HL079126 (KKP). We are grateful to the Center of Nanoscale Systems at Harvard University for the use of their cleanroom facilities, to Alexander P. Nesmith for developing the brick patterned stamps, and to Harvard SEAS Academic Computing for their support.

Appendix A. Supplementary data

Supplementary data associated with this article can be found in the online version at doi:10.1016/j.jbiomech.2011.11.024.

References

Alford, P.W., Feinberg, A.W., Sheehy, S.P., Parker, K.K., 2010. Biohybrid thin films for measuring contractility in engineered cardiovascular muscle. Biomaterials 31 (13), 3613–3621.
Anand, L., 1996. A constitutive model for compressible elastomeric solids. Computational Mechanics 18 (5), 339–355.
Atkinson, A., 1995. British Ceramic Proceedings 54 (1).
Blemker, S.S., Pinsky, P.M., Delp, S.L., 2005. A 3D model of muscle reveals the causes of nonuniform strains in the biceps brachii. Journal of Biomechanics 38, 657–665.
Böl, M., Reese, S., 2008. Micromechanical modelling of skeletal muscles based on the finite element method. Computer Methods in Biomechanics and Biomedical Engineering 11, 489–504.
Böl, M., Reese, S., Parker, K.K., Kuhl, E., 2009. Computational modeling of muscular thin film for cardiac repair. Computational Mechanics 43, 535–544.
Brown, S.B., Kim, K.H., Anand, L., 1989. An internal variable constitutive model for hot-working of metals. International Journal of Plasticity 5 (2), 95–130.
Calvo, B., Ramirez, A., Alonso, A., Grasa, J., Soteras, F., Osta, R., Munoz, M.J., 2010. Passive nonlinear elastic behaviour of skeletal muscle: experimental results and model formulation. Journal of Biomechanics 43, 318–325.
Chapelle, D., Gerbeau, J.F., Sainte-Marie, J., Vignon-Clementel, I.E., 2010. A poroelastic model valid in large strains with applications to perfusion in cardiac modeling. Computational Mechanics 46, 91–101.
Engler, A.J., Carag-Krieger, C., Johnson, C.P., Raab, M., Tang, H.-Y., Speicher, D.W., Sanger, J.W., Sanger, J.M., Discher, D.E., 2008. Embryonic cardiomyocytes beat best on a matrix with heart-like elasticity: scar-like rigidity inhibits beating. Journal of Cell Science 121, 3794–3802.
Feinberg, A.W., Feigel, A., Shevkoplyas, S.S., Sheehy, S., Whitesides, G.M., Parker, K.K., 2007. Muscular thin films for building actuators and powering devices. Science 317 (5843), 1366–1370.
Granzier, H.L., Irving, T.C., 1995. Passive tension in cardiac muscle: contribution of collagen, titin, microtubules, and intermediate filaments. Biophysical Journal 68, 1027–1044.
Griffin, M.A., Engler, A.J., Barber, T.A., Healy, K.E., Sweeney, H.L., 2004. Patterning, prestress, and peeling dynamics of myocytes. Biophysical Journal 86, 1209–1222.

Gurtin, M.E., Fried, E., Anand, L., 2010. The Mechanics and Thermodynamics of Continua. Cambridge University Press, New York.
Kroner, E., 1960. Allgemeine kontinuums theorie der versetzungen und eigenspannungen. Archive for Rational Mechanics and Analysis 4, 273–334.
Lee, E.H., 1969. Elastic–plastic deformation at finite strains. Journal of Applied Mechanics 36, 1.
Nishimura, S., Yasuda, S., Katoh, M., Yamada, K.P., Yamashita, H., Saeki, Y., Sunagawa, K., Nagai, R., Hisada, T., Sugiura, S., 2000. Single cell mechanics of rat cardiomyocytes under isometrica unloaded and physiologically loaded conditions. AJP—Heart and Circulatory Physiology 287, H196–H202.
Palmer, R.E., Brady, A.J., Roos, K.P., 1996. Mechanical measurements from isolated cardiac myocytes using a pipette attachment system. AJP—Cell Physiology 270, C697–C704.
Place, E.S., Evans, N.D., Stevens, M.M., 2009. Complexity in biomaterials for tissue engineering. Nature Materials 8 (6), 457–470.
Sainte-Marie, J., Chapelle, D., Cimrman, R., Sorine, M., 2006. Modeling and estimation of the cardiac electromechanical activity. Computers and Structures 84, 1743–1759.
Sermesant, M., Moireau, P., Camara, O., Sainte-Marie, J., Andriantsimiavona, R., Cimrman, R., Hill, D.L.G., Chapelle, D., Razavi, R., 2006. Cardiac function estimation from MRI using a heart model and data assimilation: advances and difficulties. Medical Image Analysis 10, 642–656.
Spencer, A.J.M., 1984. Continuum Theory of the Mechanics of Fibre-reinforced Composites. Springer-Verlag, Wien-New York.
Stoney, G.G., 1909. The tension of metallic films deposited by electrolysis. Proceedings of the Royal Society of London A 82, 172–175.
Wang, N., Tolic-Norrelykke, I.M., Chen, J., Mijailovich, S.M., Butler, J.P., Fredberg, J.J., Stamenovic, D., 2002. Cell prestress. I. Stiffness and prestress are closely associated in adherent contractile cells. AJP—Cell Physiology 282, C606–C616.
Weiss, J.A., Marker, B.N., Govindjee, S., 1996. Finite element implementation of incompressible, transversely isotropic hyperelasticity. Computer Methods in Applied Mechanics and Engineering 135, 107–128.
Weiwad, W.K.K., Linke, W.A., Wussling, M.H.P., 2000. Sarcomere length–tension relationship of rat cardiac myocytes at lengths greater than optimum. Journal of Molecular and Cellular Cardiology 32, 247–259.

Supporting Material for Modeling of Cardiac Muscular Thin Films: Pre-stretch, Passive and Active Behavior

Jongmin Shim[1], Anna Grosberg[2], Janna C. Nawroth[3], Kevin Kit Parker[2], and Katia Bertoldi[1]

[1]*School of Engineering and Applied Science, Harvard University, Cambridge, MA*
[2]*Disease Biophysics Group, Wyss Institute for Biologically Inspired Engineering, School of Engineering and Applied Science, Harvard University, Cambridge, MA*
[3]*Division of Biology, California Institute of Technology, Pasadena, CA*

S1 Experimental Methods

This section provides a detailed description of the preparation of the silicone thin film and cell harvesting procedure.

S1.1 Manufacturing the Silicone Thin Films

The silicone thin films were prepared via a multi-step spin coating process, extending a previously published method (Feinberg et al., 2007) in order to allow for higher experimental throughput. The samples prepared this way have been dubbed "Heart on a chip". To prepare the chips, a section of glass ($7.5cm \times 11cm$) was sonicated and covered with a protective film (Static Cling Film, McMaster-Carr, Robbinsville, NJ) on both sides. Rectangles ($1cm \times 0.6cm$) were cut out of the top protective film, and poly(N-isopropylacrylamide) (PIPAAm, Polysciences, Inc., Warrington, PA) in 1-butanol (10% w/v) was spin-coated onto the uncovered portions of the glass, and then the top protective film was removed. The silicone polymer polydimethylsiloxane (PDMS, Sylgard 184-Dow Corning, Midland, MI) was pre-cured for 1 to 6 hours, spin coated onto the glass, and cured for 8 hours at $65°C$. The bottom protective film was removed, and the glass section was cut into cover slips of $1.4cm \times 1.2cm$. From each glass section, two cover slips were used to measure the thickness of the PDMS layer using a profilometer (Dektak 6M, Veeco Instruments Inc., Plainview, NY). The PDMS surface of the cover slip was functionalized and sterilized for 8 minutes in UV ozone (Model No. 342, Jetlight Company, Inc., Phoenix, AZ). Fibronectin (FN, Sigma, St. Louis, MO or BD Biosciences, Sparks, MD) was micropatterned onto the surface via microcontact printing with a brick pattered PDMS stamp (each brick was $20\mu m$ wide and $100\mu m$ long, and each short edge terminated with $5\mu m$ long saw-tooth, Bray et al., 2008), such that the brick pattern would be perpendicular or at some tilted angle to the long edge of the cover slip. The gaps in the pattern were blocked by incubating the cover slip in Pluronics F127 (BASF Group, Parsippany, NJ) for 5 minutes, and then the chips were stored at $4°C$ until cell seeding. Three different PDMS thickness were made though this procedure: $14.5\mu m$, $18.0\mu m$, $23.0\mu m$.

S1.2 Cell harvesting, Seeding, and Culture

Cell harvesting was conducted in accordance with the guidelines of Institutional Animal Care and Use Committee of Harvard University. Cardiomyocytes were harvested and isolated based on published protocols (Adams et al., 2007). Briefly, ventricles were extracted from two-day-old neonatal Sprague-Dawley rats (Charles River Laboratories, Wilmington, MA) and homogenized by washing in Hanks balanced salt solution, then incubated with trypsin overnight at $4°C$. To release the myocytes into solution, the ventricular tissue was digested with collagenase at $37°C$. Cells were re-suspended in M199 culture medium supplemented with 10% (v/v) heat-inactivated fetal bovine serum (FBS), $10mM$ HEPES, $3.5g/L$ glucose, $2mM$ L-glutamine, $2mg/L$ vitamin B-12, and $50U/ml$ penicillin. The myocytes were seeded on the substrates at a density of 400,000 cells per cover slip (round, diameter of $18mm$), and cultured for a period of four days prior to running the assay. During the initial 48 hours, the cells were kept at $37°C$ and $5\%CO_2$ with 10% FBS media in the culture; thereafter, the maintenance media (2% FBS) was used. The measured cell thickness was approximately $4.0\mu m$.

S1.3 Contractility Experiments

To run the contractility experiments, the chip was moved to a Petri dish with $37°C$ normal Tyrode's solution ($1.192g$ of HEPES, $0.901g$ of glucose, $0.265g$ of $CaCl_2$, $0.203g$ of $MgCl_2$, $0.403g$ of KCl, $7.889g$ of $NaCl$, and $0.040g$ of NaH_2PO_4 per liter of deionized water; reagents from Sigma, St. Louis, MO). The PDMS elastic layer was cut such as to leave the PDMS along the border of the cover slip intact, while in the center there were two rows of three to four rectangles (approximately $2mm \times 3.5mm$) separated by approximately $1mm$, and connected to the PDMS border by one edge (see Fig. 2A). The unwanted film was peeled away, exposing the temperature-sensitive PIPAAm beneath the rectangular strips and causing it to dissolve as the solution was allowed to cool down towards room temperature. Subsequently, the rectangular films were free to move vertically up from the plane of the cell culture, without completely separating from the chip. The chip with six or eight rectangular films was moved to a heated bath ($34°C - 37°C$) under a stereomicroscope (Model MZ6 with darkfield base, Leica Microsystems, Inc., Wetzlar, Germany), and the dynamics of the films was recorded from above at 120 $frames/sec$ (Basler A602f camera, Exton, PA). Several snapshots from the recorded movies are shown in Figs. 2A and 2E.

While the film laid flat on the glass, both its length and width were measured. As the films contracted away from the surface, the horizontal projection was recorded. Unimpeded films would first isometrically deform to a curvature corresponding to the diastolic tension in the cells, and then continue to deform until peak systole. For substrates with cells aligned with the length of the film, the observed deformation was a shortening of the projection, described in Fig. 1C (top). On the other hand, the substrates with cells at an angle to the length of the film showed the inclined free edge of the film (see Fig. 1C (bottom)), so an appropriate projection length needed to be defined in order to obtain the curvature of the MTFs. To ensure all films on the chip were moving at once, the myocytes were field-stimulated at $1.5Hz$ with 5 to $20V$ using an external field stimulator (Myopacer, IonOptix Corp., Milton, MA) which applied a $10msec$ square wave pulse.

S2 Constitutive Equations for Bio-hybrid Films

In this section, we first summarize the equations governing the nonlinear deformation of hyperelastic materials, following the formulation previously introduced by Bergström and Boyce (1998). Then, the equations are specialized to capture the behavior of the elastomeric substrate and the cardiac myocytes. As mentioned in Section 1, cardiac myocytes comprise highly aligned myofibrils, so their behavior is captured extending the formulation previously developed to model fiber reinforced elastomers (Spencer, 1984).

S2.1 General Formulation

Let $\mathbf{F} = \partial\mathbf{x}/\partial\mathbf{X}$ be the deformation gradient mapping a material point from the reference position $\mathbf{X}$ to its current position $\mathbf{x}$, and $J = \det\mathbf{F}$ be its determinant. The behavior of nearly incompressible materials is effectively described by splitting the deformation locally into volumetric (denoted by superscript v) and isochoric (denoted by superscript i) components as

$$\mathbf{F} = \mathbf{F}^v \cdot \mathbf{F}^i, \quad \text{where} \quad \mathbf{F}^v = J^{1/3}\mathbf{1}, \quad \mathbf{F}^i = J^{-1/3}\mathbf{F}. \tag{S1}$$

For an isotropic hyperelastic material, the strain energy density ψ is a function of the three invariants of $\mathbf{C} = \mathbf{F}^T \cdot \mathbf{F}$, $\psi = \psi(I_1, I_2, I_3)$. Based on the kinematic assumption (S1), a decoupled

form for ψ is introduced

$$\psi = \psi^v(J) + \psi^i(\bar{I}_1, \bar{I}_2), \tag{S2}$$

with

$$\bar{I}_1 = \mathrm{tr}\mathbf{C}^i, \quad \bar{I}_2 = \frac{1}{2}\left[\left(\mathrm{tr}\mathbf{C}^i\right)^2 - \mathrm{tr}\left(\mathbf{C}^{i^2}\right)\right]. \tag{S3}$$

When an isotropic material is reinforced by a family of fibers with direction $\mathbf{a}_0$ in the reference configuration, the isochoric part of the strain energy can be expressed as a function of not only $\bar{I}_1$ and $\bar{I}_2$, but also two additional invariants $(\bar{I}_4, \bar{I}_5)$ depending on $\mathbf{a}_0$ (Spencer, 1984),

$$\psi^i = \psi^i(\bar{I}_1, \bar{I}_2, \bar{I}_4, \bar{I}_5), \tag{S4}$$

with

$$\bar{I}_4 = \mathbf{a}_0 \cdot \mathbf{C}^i \cdot \mathbf{a}_0 = \bar{\lambda}^2, \quad \bar{I}_5 = \mathbf{a}_0 \cdot \mathbf{C}^{i^2} \cdot \mathbf{a}_0. \tag{S5}$$

However, the dependence of the material response on $\bar{I}_2$ or $\bar{I}_5$ is generally weak, so that the isochoric part of the strain energy can be simplified as

$$\psi^i = \psi^i_{iso}\left(\bar{I}_1\right) + \psi^i_{ani}\left(\bar{I}_4\right), \tag{S6}$$

where ψ^i is further decoupled into the isotropic contribution (ψ^i_{iso}) and the anisotropic contribution (ψ^i_{ani}).

Finally, the Cauchy stress $\mathbf{T}$ is found by differentiating ψ with respect to $\mathbf{C}$ as

$$\mathbf{T} = \frac{2}{J}\mathbf{F}\frac{\partial \psi}{\partial \mathbf{C}}\mathbf{F}^T = \frac{\partial \psi^v}{\partial J}\mathbf{1} + \frac{2}{J}\left[\frac{\partial \psi^i_{iso}\left(\bar{I}_1\right)}{\partial \bar{I}_1}\mathrm{dev}\left(\mathbf{B}^i\right) + \bar{I}_4\frac{\partial \psi^i_{ani}\left(\bar{I}_4\right)}{\partial \bar{I}_4}\mathrm{dev}\left(\bar{\mathbf{a}} \otimes \bar{\mathbf{a}}\right)\right], \tag{S7}$$

where "dev" stands for deviatoric part of 2^{nd} order tensors, $\mathbf{B}^i = \mathbf{F}^i \cdot \mathbf{F}^{iT}$ is the left Cauchy-Green tensor, and $\bar{\mathbf{a}} = \mathbf{F}^i \cdot \mathbf{a}_0/\sqrt{\bar{I}_4}$ is the unit directional vector of fiber in the deformed configuration. In the following two sections, the above general formulation is specialized to capture the behavior of the elastomeric substrate and the cardiac myocytes.

S2.2 Elastomeric Substrate

The elastomeric substrate is fabricated using PDMS, and its behavior is well captured using a neo-Hookean model. A decoupled form of strain energy density is given by:

$$\psi = \psi^v\left(J\right) + \psi^i\left(\bar{I}_1\right) = \frac{\tilde{\kappa}}{2}\left(J-1\right)^2 + \frac{\tilde{E}}{6}\left(\bar{I}_1 - 3\right), \tag{S8}$$

where $\tilde{\kappa}$ and $\tilde{E}$ denote the bulk modulus and the initial elastic modulus of the elastomer, respectively. Based on Eq. (S7), the Cauchy stress is obtained as:

$$\mathbf{T} = \tilde{\kappa}(J-1)\mathbf{1} + \frac{\tilde{E}}{3J}\mathrm{dev}\left(\mathbf{B}^i\right). \tag{S9}$$

S2.3 Cardiac Muscle Cell

This paper presents a 3-D phenomenological model that captures the two major features of cardiac muscles: the passive behavior including pre-stretched deformation and their active behavior including systole and diastole. This subsection presents a detailed derivation of the constitutive equations for the passive and active behavior while the kinematics including pre-stretch is provided in Section 3.2.

In order to describe both passive (representing resting status) and active (including systole and diastole) behavior of cardiomyocytes, we specify a decoupled from of free energy as:

$$\psi = \psi^v\left(J\right) + \psi^i_{iso}\left(\bar{I}_1\right) + \psi^{ip}_{ani}\left(\bar{I}_4\right) + \psi^{ia}_{ani}\left(\bar{I}_4, q\right), \tag{S10}$$

where q is the activation level of cardiac muscle cells. In the present model, while ψ^v and ψ^i_{iso} reflect the volumetric and the isotropic contribution of the intercellular part, respectively, ψ^{ip}_{ani} and ψ^{ia}_{ani} represent the passive and the active contributions of anisotropic effect of the myofibril, respectively.

Here, as for the elastomeric substrate, the volumetric free energy term is chosen as

$$\psi^v(J) = \frac{\hat{\kappa}}{2}\left(J-1\right)^2, \tag{S11}$$

and the isotropic contribution of the intercellular part is captured using a neo-Hookean formulation

$$\psi^i_{iso} = \frac{\hat{E}_c}{6}\left(\bar{I}_1 - 3\right), \tag{S12}$$

where $\hat{\kappa}$ denotes the bulk modulus of the cells and $\hat{E}_c$ is the initial elastic modulus of intercellular part. Several experimental studies (Le Guennec et al., 1990; Granzier and Irving, 1995; Palmer et al., 1996; Cazorla et al., 2000; Weiwad et al., 2000; Boron and Boulpaep, 2009) reveal that the passive response of cardiac cells is characterized by an exponential relation between stress and deformation (see Fig. 3A). In order to capture such behavior of cardiac cells, we propose the following free energy

$$\psi^{ip}_{ani}\left(\bar{\lambda}\right) = \frac{\hat{E}_p}{\hat{\alpha}^2}\left[e^{\hat{\alpha}(\bar{\lambda}-1)} - \hat{\alpha}(\bar{\lambda}-1) - 1\right], \tag{S13}$$

where $\bar{\lambda} = \sqrt{\bar{I}_4}$, $\hat{E}_p$ is the initial elastic modulus, and $\hat{\alpha}$ characterizes the monotonically increasing slope of the stress-strain relation of the passive response of the fibers. For the active response (see Fig. 3B), a bell-type relation between stress and deformation was shown by several studies (Zajac, 1989; Weiwad et al., 2000; Boron and Boulpaep, 2009). Here, we simplify the active stress-stretch relation into a quadratic form, which is captured introducing the following free energy

$$\psi^{ia}_{ani}\left(\bar{\lambda}, q\right) = \begin{cases} \frac{\hat{P}q}{2(1-\hat{\lambda}_o)^2}\left[2(1-2\hat{\lambda}_o)\ln\bar{\lambda} + (4\hat{\lambda}_o - \bar{\lambda} - 1)(\bar{\lambda}-1)\right], & \text{if } 1 < \bar{\lambda} < (2\hat{\lambda}_o - 1), \\ 0, & \text{otherwise,} \end{cases} \tag{S14}$$

where $\hat{P}$ is the isometric twitch stress (*i.e.*, the maximum contraction force per unit cross-sectional area) and $\hat{\lambda}_o$ is the optimal stretch (*i.e.*, the stretch at which the maximum active stress is attained). Since Fig. 2B-D and F clearly show that diversity in cell conditions causes

large variations of the peak amplitudes, a range of values for $\hat{P}$ will be identified to account for biological variability. Finally, the activation level q is a function of time and is defined as

$$q(t) = \left(\frac{t}{\hat{T}}\right)^2 \exp\left[1 - \left(\frac{t}{\hat{T}}\right)^2\right], \tag{S15}$$

where $\hat{T}$ is the characteristic contraction time.

Based on Eq. (S7), the proposed free energy results in the following Cauchy stress

$$\mathbf{T} = \mathbf{T}^v + \mathbf{T}^i_{iso} + \mathbf{T}^{ip}_{ani} + \mathbf{T}^{ia}_{ani}, \tag{S16}$$

where

$$\mathbf{T}^v = \hat{\kappa}(J-1)\mathbf{1}, \tag{S17}$$

$$\mathbf{T}^i_{iso} = \frac{\hat{E}_c}{3J}\mathrm{dev}\left(\mathbf{B}^i\right), \tag{S18}$$

$$\mathbf{T}^{ip}_{ani} = \frac{\hat{E}_p\bar{\lambda}}{\hat{\alpha}J}\left[e^{\hat{\alpha}(\bar{\lambda}-1)} - 1\right]\mathrm{dev}(\bar{\mathbf{a}}\otimes\bar{\mathbf{a}}), \tag{S19}$$

$$\mathbf{T}^{ia}_{ani} = \begin{cases} \frac{\hat{P}q}{J}\left[1 - \left(\frac{\bar{\lambda}-\hat{\lambda}_o}{1-\hat{\lambda}_o}\right)^2\right]\mathrm{dev}(\bar{\mathbf{a}}\otimes\bar{\mathbf{a}}), & \text{if } \ 1 < \bar{\lambda} < (2\hat{\lambda}_o - 1), \\ 0, & \text{otherwise.} \end{cases} \tag{S20}$$

S3 Parameter Identification for the Constitutive Model

This section presents the procedure to identify the 11 material parameters entering into the proposed 3-D constitutive model. While the material parameters for the elastomeric substrate are provided by the manufacturers, the parameters needed for the cardiac muscle cell response are obtained from literature and contraction assays performed with neonatal rat ventricular myocytes micropatterned on PDMS thin films.

S3.1 Summary of Model Parameters

The proposed constitutive model requires 11 material constants:

- Elastomeric substrate
  $\tilde{E}$ Initial elastic modulus
  $\tilde{\kappa}$ Initial bulk modulus

- Pre-stretched deformation of cardiac muscle cells
  $\hat{\theta}$ Angle defining the initial alignment of the cells within the $x_1 - x_2$ plane
  $\hat{\lambda}_S$ Pre-stretch developed in the cardiomyocytes during cell maturation

- Volumetric and isotropic behavior of cardiac muscle cells
  $\hat{E}_c$ Initial elastic modulus of intercellular part
  $\hat{\kappa}$ Initial bulk modulus

- Passive fiber behavior of cardiac muscle cells
  $\hat{E}_p$ Initial elastic modulus of fiber
  $\hat{\alpha}$ Constant related to the slope of stress-strain relation of passive fiber

- Active fiber behavior of cardiac muscle cells
  $\hat{P}$ Isometric twitch stress
  $\hat{\lambda}_o$ Optimal stretch for the maximum active stress
  $\hat{T}$ Characteristic time scale for contraction

S3.2 Elastomeric Substrate ($\tilde{E}$, $\tilde{\kappa}$)

Only two material constants ($\tilde{E}$, $\tilde{\kappa}$) are required to model the elastomeric substrates. The initial elastic modulus is directly specified by the manufacturer as $\tilde{E} = 1.5MPa$, while its incompressible behavior ($\tilde{\nu} = 0.49$) yields an initial bulk modulus of $\tilde{\kappa} = \frac{\tilde{E}}{3(1-2\tilde{\nu})} = 25MPa$.

S3.3 Cardiac Myocytes

The proposed model requires seven material-specific parameters ($\hat{\kappa}$, $\hat{E}_c$, $\hat{E}_p$, $\hat{\alpha}$, $\hat{P}$, $\hat{\lambda}_o$, $\hat{T}$) and two geometric-specific parameters ($\hat{\theta}$, $\hat{\lambda}_S$). Most of model parameters are available in the literature. The paper by Weiwad et al. (2000) provides in a single article nearly all the required test results to identify the material parameters entering into the proposed material model. Moreover, all their data are in a good agreement with similar test results for the heart muscle of adult rats (Granzier and Irving, 1995, Palmer et al., 1996 for passive behavior and Nishimura et al., 2000, Palmer et al., 1996 for active behavior). Thus, the test results presented in Weiwad et al. (2000) are used to identify five material-specific parameters entering into the proposed constitutive model.

In addition, experiments with length-wise cell alignment (Section 2) are used to identify the remaining three parameters; two experimental-conditions-specific parameters ($\hat{P}$, $\hat{\lambda}_S$) and the characteristic time scale of contractile behavior under the stimulating electric pulse ($\hat{T}$). Here, we assume that the cell conditions affect only the twitch stress $\hat{P}$ and the pre-stretch $\hat{\lambda}_S$.

Isochoric Behavior of Intercellular Part ($\hat{E}_c$) and Isochoric Passive Behavior of Fiber Part ($\hat{E}_p$, $\hat{\alpha}$) Several researchers reported experimentally measured values for Young's modulus of non-activated rat cardiac myocytes by using atomic force microscopy (Lieber et al., 2004) or custom-designed force transducer (Weiwad et al., 2000). The measured values vary from $20kPa$ to $45kPa$ depending on the experimental protocols and the ages of rats. Following Weiwad et al. (2000), we use a Young's modulus, $\hat{E}_{passive} = 23kPa$ (see Fig. 3A). From Eq. (S16), recall that the measured Young's modulus of the non-activated cell can be decomposed into the contribution of intercellular part and passive fiber part. Here, we assume that the passive fiber part is mainly responsible for the passive elastic behavior, so that $\hat{E}_p = 21kPa$ and $\hat{E}_c = 2.3kPa$. Note that the passive stress ($T_{11}^{passive}$) can be expressed as:

$$T_{11}^{passive} = \left(T_{iso}^{i}\right)_{11} + \left(T_{ani}^{ip}\right)_{11}, \tag{S21}$$

where using incompressibility each stress contribution can be determined from Eq. (S18) and Eq. (S19) assuming uniaxial loading conditions:

$$\left(T_{iso}^{i}\right)_{11} = \frac{\hat{E}_c}{3}\left(\bar{\lambda}^2 - \frac{1}{\bar{\lambda}}\right), \tag{S22}$$

$$\left(T_{ani}^{ip}\right)_{11} = \frac{\hat{E}_p\bar{\lambda}}{\hat{\alpha}}\left[e^{\hat{\alpha}(\bar{\lambda}-1)} - 1\right]. \tag{S23}$$

By curve-fitting the experimental results with the above equations (see Fig. 3B), we obtain $\hat{\alpha} = 5.5$.

Isochoric Active Behavior of Fiber Part ($\hat{P}$, $\hat{\lambda}_o$, $\hat{T}$) Weiwad et al. (2000) reported the evaluation of the isometric twitch stress as a function of calcium concentration (see Fig. 3B). Note that a constant calcium concentrations of $pCa = -log_{10}(a_{Ca^{2+}}) = 2.74$ was used throughout the essay tests (Fig. 2) presented in Section 2. In order to get its overall dependence on the stretch, all the active tension-stretch relations are normalized by its maximum value, and then curve-fitted by the proposed quadratic form of active stress-stretch relation specialized to uniaxial loading:

$$\left(T^{ia}_{ani}\right)_{11} = \begin{cases} \hat{P}q\left[1 - \left(\frac{\bar{\lambda}-\hat{\lambda}_o}{1-\hat{\lambda}_o}\right)^2\right], & \text{if } 1 < \bar{\lambda} < (2\hat{\lambda}_o - 1) \\ 0, & \text{otherwise} \end{cases} \tag{S24}$$

As a result, we obtain $\hat{\lambda}_o = 1.24$, as shown in Fig. 3B. As described in Section 4, a range of values for the isometric twitch stress of $\hat{P} \in [2.8,\ 21.6]kPa$ is determined from experiments with length-wise cell alignment presented in Section 2. The characteristic contraction time can be determined by measuring the time when the signal reaches its maximum value after the activation starts. Fig. 3C shows a typical profile of the active amplitude history, and $\hat{T} = 0.21sec$ is determined.

Volumetric Behavior ($\hat{\kappa}$) For simplicity, we assume that the cardiac muscle is nearly incompressible and its volumetric behavior is determined by the passive response. Thus, using $\hat{E}_{passive} = 23kPa$ and $\hat{\nu} = 0.49$, we obtain a bulk modulus of $\hat{\kappa} = \frac{\hat{E}_{passive}}{3(1-2\hat{\nu})} = 380kPa$.

Isochoric Pre-stretch Behavior ($\hat{\theta}$, $\hat{\lambda}_S$) For the model parameter identification, the controlled test set (*i.e.*, the case with the length-wise cell alignment) with $\hat{\theta} = 0^\circ$ is used.

From the assay experiments in Section 2, we obtain $\hat{\lambda}_S \in [1.11, 1.18]$. Similar range of values for pre-stretch was also reported using a silicon substrate (Mansour et al., 2004).

S4 Parametric Studies

In this Section, we explore the effect of important parameters within MTFs with length-wise cell alignment such as the PDMS thickness, the isometric twitch stress of cells, the pre-stretch of cells, and the frequency of field-stimulation.

Effect of PDMS Thickness Here, the effect of PDMS thickness on the response of the MTFs is explored by varying $\tilde{t}$ from $13.0\mu m$ to $28.0\mu m$. The average value of the two cell-condition-dependent parameters is used (*i.e.*, $\hat{\lambda}_S = 1.14$ and $\hat{P} = 9.0kPa$), while keeping all other parameters unchanged.

Fig. S1A shows the effect of PDMS thickness on the total curvature (K) of MTFs. As expected, an increase in PDMS thickness leads to a decrease in curvature. To quantify this behavior, the total curvature is decomposed into the passive contribution (K_p) and the active contribution (K_a):

$$K = K_p + K_a. \tag{S25}$$

Fig. S1B reports the evolution of maximum passive and active curvature contributions (*i.e.*, $max(K_p)$ and $max(K_a)$) as a function of the PDMS thickness. The passive contribution of the curvature can be also estimated by applying a recent modification of the Stoney's equation

(Atkinson, 1995). Assuming that the layer of cells is much thinner than that of substrate, the Stoney *curvature* equation predicts the curvature of the bilayer film as

$$K_{stoney} = \frac{6(\hat{E}_c + \hat{E}_p)\ \ln\hat{\lambda}_S}{\tilde{E}\tilde{t}} \left(\frac{\hat{t}}{\tilde{t}}\right) \left(1 + \frac{\hat{t}}{\tilde{t}}\right). \tag{S26}$$

The pre-stretched curvature predicted by (S26) is also reported in Fig. **??**, and a good agreement with the passive contribution from the FEM calculations is observed.

Effect of Isometric Twitch Stress of Cells We vary $\hat{P}$ from 0 to $30.0kPa$ while keeping all other parameters unchanged, including $\tilde{t} = 18.0\mu m$ and $\hat{\lambda}_S = 1.14$.

Fig. S1C shows the effect of isometric twitch stress on the curvature of MTFs. While the passive contribution of the curvature ($max(K_p)$) is unaffected by $\hat{P}$, the active contribution ($max(K_a)$) is observed to vary almost linearly with $\hat{P}$ (Fig. S1D).

Effect of Cell Pre-stretch The effect of pre-stretch on the cardiomyocyte response is investigated by varying $\hat{\lambda}_S$ from 1.00 (*i.e.*, no pre-stretch) to 1.39 while keeping all other parameters unchanged and using $\tilde{t} = 18.0\mu m$ and $\hat{P} = 9.0kPa$.

Figure S1E reports the time history of film curvature for various level of cell pre-stretch. The results clearly show that the level of cell pre-stretch affects the curvature both during cell maturation and activation. Interestingly, for the active response, we observe a quadratic relation between the passive and the active curvature contribution. Thus, this study suggests that the maximum level of active response (*i.e.*, the maximum active mobility) for the MTFs can be achieved by introducing an optimal pre-stretch value. Moreover, Fig. S1F clearly show that the modified Stoney equation (*i.e.*, Eq. (S26)) largely underestimates the MTF curvature for large pre-stretch.

References

W.J. Adams, T. Pong, N.A. Geisse, S.P. Sheehy, B. Diop-Frimpong, and K.K. Parker. Engineering design of a cardiac myocyte. *Journal of Computer-Aided Materials Design*, 14(1):19–29, 2007.

A. Atkinson. *British Ceramic Proceedings*, 54(1), 1995.

J.S. Bergström and M.C. Boyce. Constitutive modelling of the large strain time-dependent behavior of elastomers. *Journal of the Mechanics and Physics of Solids*, 46:931–954, 1998.

W.F. Boron and E.L. Boulpaep. *Medical Physiology*. Saunders, 2009.

M.A. Bray, S.P. Sheehy, and K.K. Parker. Sarcomere alignment is regulated by myocyte shape. *Cell Motility and the Cytoskeleton*, 65(8):641–651, 2008.

O. Cazorla, J.-Y. Le Guennec, and E. White. Lenght-tension relationships of sub-epicaridal and sub-endocardial single ventricular myocytes from rat and ferret hearts. *Journal of Molecular and Cellular Cardiology*, 32:735–744, 2000.

A.W. Feinberg, A. Feigel, S.S. Shevkoplyas, S. Sheehy, G.M. Whitesides, and K.K. Parker. Muscular thin films for building actuators and powering devices. *Science*, 317(5843):1366–1370, 2007.

H.L. Granzier and T.C. Irving. Passive tension in cardiac muscle: contribution of collagen, titin, microtubules, and intermediate filaments. *Biophysical Journal*, 68:1027–1044, 1995.

J.-Y. Le Guennec, N. Peineau, J.A. Argibay, K.G. Mongo, and D. Garnier. A new method of attachment of isolated mamalian ventricular myocytes for tension recording: Length dependence of passive and active tension. *Journal of Molecular and Cellular Cardiology*, 22: 1083–1093, 1990.

S.C. Lieber, N. Aubry, J. Pain, G. Diaz, S.J. Kim, and S.F. Vatner. Aging increases stiffness of cardiac myocytes measured by atomic force microscopy nanoindentation. *AJP-Heart and Circulatory Physiology*, 287:H645–H651, 2004.

H. Mansour, P.P. de Tombe, A.M. Samarel, and B. Russell. Restoration of resting sarcomere length after uniaxial static strain is regulated by protein kinase cϵ and focal adhesion kinase. *Circulation Research*, 94:642–649, 2004.

S. Nishimura, S. Yasuda, M. Katoh, K.P. Yamada, H. Yamashita, Y. Saeki, K. Sunagawa, R. Nagai, T. Hisada, and S. Sugiura. Single cell mechanics of rat cardiomyocytes under isometric, unloaded, and physiologically loaded conditions. *AJP-Heart and Circulatory Physiology*, 287: H196–H202, 2000.

R.E. Palmer, A.J. Brady, and K.P. Roos. Mechanical measurements from isolated cardiac myocytes using a pipette attachment system. *AJP-Cell Physiology*, 270:C697–C704, 1996.

A.J.M. Spencer. *Continuum Theory of the Mechanics of Fibre-reinforced Composites*. Springer-Verlag, Wien-New York, 1984.

W.K.K. Weiwad, W.A. Linke, and M.H.P. Wussling. Sarcomere length-tension relationship of rat cardiac myocytes at lengths greater than optimum. *Journal of Molecular and Cellular Cardiology*, 32:247–259, 2000.

F.E. Zajac. Muscle and tendon: Properties, models, scaling, and application to biomechanics and motor control. *Critical Reviews in Biomedical Engineering*, 17:359–411, 1989.

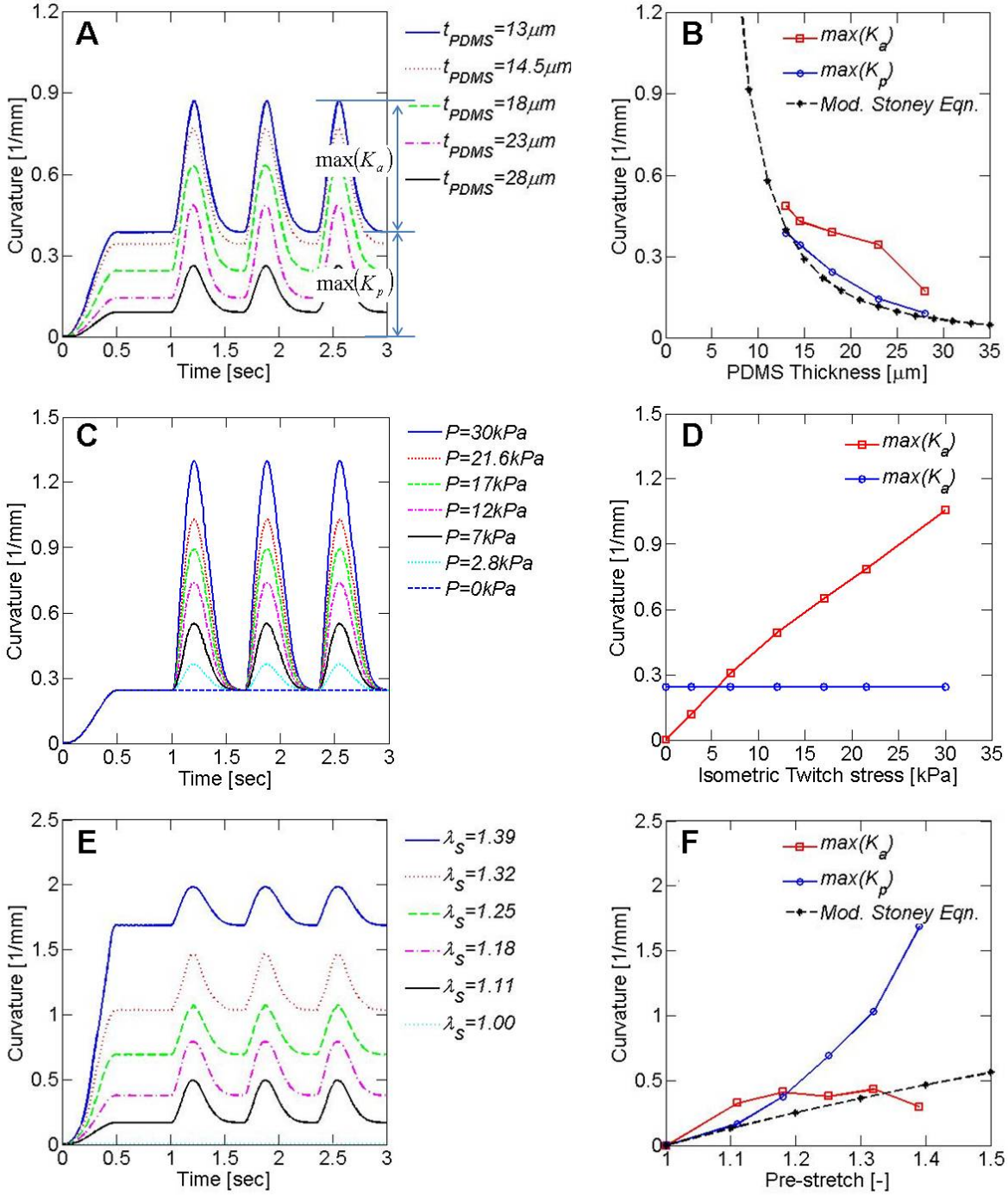

Figure S1: FE parametric studies: the left column for the time-curvature plots from FE analysis, and the right column for the curvature contribution of passive and active response ($max(K_p)$ and $max(K_a)$). (A-B) effect of PDMS thickness, (C-D) Effect of isometric twitch stress of cells, (E-F) effect of cell pre-stretch.